# Laboratory Simulation of Seamless Tube Piercing and Rolling Using Dynamic Recrystallization Schedules

L.N. PUSSEGODA, S. YUE, and J.J. JONAS

A seamless tube mill rolling process was simulated with the aim of designing alloys and schedules for the production of as-hot-rolled yield strength levels which are currently attained only by quenching and tempering. Tests were performed on four candidate Ti-V-N steels with two levels each of carbon (0.10 and 0.18 wt pct) and vanadium (0.10 and 0.16 wt pct). Two different types of schedule were used: (1) a high-temperature schedule, corresponding to the production of large tube diameters, which utilizes the principles of recrystallization-controlled rolling (RCR) and (2) a second (for small tubes), which relies on *dynamic* recrystallization-controlled rolling (DRCR). The DRCR schedule, together with the higher cooling rate achievable on the smaller tube sizes, produces a much finer ferrite grain size than the RCR schedule. However, this is largely offset by increased strengthening in the RCR structure *via* precipitation hardening. As-hot-rolled yield strengths in the range of 483 to 715 MPa (70 to 104 ksi) can be achieved using either type of schedule.

## I. INTRODUCTION

THERMOMECHANICAL processing techniques have been applied extensively to control the final microstructure and, therefore, the mechanical properties of microalloyed plate and strip steels. The economic benefits resulting from the elimination of post-hot-rolling treatments are well known. These concepts are also applicable to other shapes, and such methods are gaining acceptance in the manufacture of rounds, bars, and forgings.[1,2,3] The present work is part of a continuing project[4,5] concerning the application of microalloying methods to the production of seamless tubes.

Rolling in the #2 seamless tube mill of the Algoma Steel Corporation, Sault Ste. Marie, ON, Canada, is carried out in three main stages: piercing, retained mandrel mill rolling (the MPM stage), and stretch reducing (the SRM stage).[6] The rolling schedule employed in this process is similar to many other steel-rolling schedules in that it can be divided into a high-temperature or roughing stage (piercing and MPM) and a low-temperature or finishing stage (SRM). However, the seamless schedule is unusual in that an intermediate reheat furnace is employed between the MPM and SRM stages. Such an intermediate reheat can be used to produce grain refinement by cooling below the austenite-to-ferrite transformation temperature ($A_{r1}$) prior to reheating to the usual finish-rolling temperature of about 1000 °C.

The specific rolling schedule depends primarily on the final tube size. Two extremes, corresponding to the largest (L) and smallest (S) sizes made at Algoma, were investigated in this work. The L size undergoes no SRM rolling (finishing), whereas a strain of about 1.6 is applied to the S size during finishing. The L schedule is typical of recrystallization-controlled rolling (RCR) and relies in austenite grain refinement *via* repeated cycles of recrystallization.[7] By contrast, the S schedule, which involves relatively low temperatures and very short interpass times, leads to the initiation of dynamic recrystallization[8] and is thus based on *dynamic* recrystallization-controlled rolling (DRCR).

Because recrystallization is a key component of both schedules, a conventional Nb microalloyed steel, in which recrystallization is heavily retarded, is unsuitable for this purpose. Instead, a series of Ti-V-N steels specifically designed for recrystallization-controlled rolling[4,5,9] was selected for this investigation. In these alloys, TiN precipitates prevent austenite grain growth during and after rolling, and subsequent V(CN) precipitation in the ferrite produces precipitation hardening.[9]

## II. EXPERIMENTAL PROCEDURE

Industrial rolling schedules can be readily simulated in the laboratory by means of torsion testing. In such simulations, the key hot-working variables are the strain, strain rate, temperature, and interpass time. This method has been employed successfully for the design of reversing[10,11,12] and strip mill[8,13] schedules.

### A. *Test Schedules*

The mill rolling variables for the S and L sizes were simplified into test schedules which could be simulated on the torsion apparatus. These simplified schedules are presented in Tables I and II, respectively. The equivalent strain per pass was determined from the von Mises relation:

$$\varepsilon_{eq} = \frac{\sqrt{2}}{3}[(\varepsilon_l - \varepsilon_t)^2 + (\varepsilon_t - \varepsilon_c)^2 + (\varepsilon_c - \varepsilon_l)^2]^{1/2}$$

where $\varepsilon_l$, $\varepsilon_t$, and $\varepsilon_c$ are the true principal strains. For the tube-making process, ignoring redundant strains, these three quantities correspond to the longitudinal, $l$, thickness, $t$, and circumferential, $c$, strains.[14] The temperature profile, which is the most important variable during

L.N. PUSSEGODA, Associate Professor, is with the Department of Mechanical Engineering, University of Peradeniya, Peradeniya, Sri Lanka. S. YUE, Assistant Professor, and J.J. JONAS, CSIRA-NSERC Professor of Steel Processing, are with the Department of Metallurgical Engineering, McGill University, 3450 University Street, Montreal, PQ, Canada H3A 2A7.

Manuscript submitted June 12, 1989.

**Table I. S Simulation**

| Pass No. | Equivalent Strain per Pass | Temperature (°C) | Delay Time between Passes (s) |
|---|---|---|---|
| 1—piercer | 1.60 | 1230 | 54 |
| 2—MPM | 0.45 | 1085 | 1 |
| 3—MPM | 0.40 | 1072 | 1 |
| 4—MPM | 0.30 | 1060 | 0.5 |
| 5—MPM | 0.20 | 1050 | 0.5 |
| 6—MPM | 0.18 | 1020 | 30 |
| — | — | 843 | 25 |
| — | — | 731 | — |
| Tube furnace | — | 1000 | 5 |
| 7 to 22—SRM | 0.10 | 1000 to 800 | 0.5 |

Note: Soaking temperature is 1250 °C for 15 min. Delay time between billet reheating furnace and piercer is 80 s. The strain rate is 2 $s^{-1}$ for each pass.

rolling, was for the most part faithfully reproduced in both cases. However, due to cooling rate limitations in the torsion machine furnace, the finishing temperature of ~800 °C in the S simulation could not be attained. Therefore, the lowest finishing temperature employed was ~840 °C.

The S schedule (Table I) can be clearly divided into two temperature regions. The piercing and MPM stages (passes 1 through 6) are carried out at high temperatures, while the SRM deformation (passes 7 through 22) is applied at lower temperatures. It should be noted that the tube shells cool to a minimum of ~680 °C before being reheated to 1000 °C in the tube furnace. Since the calculated $A_{r3}$ temperatures range from 737 °C to 717 °C for the steel chemistries investigated,[15] the specimens routinely cool about 50 °C below the $A_{r3}$ in the S schedule. (Although the exact as-deformed $A_{r1}$ temperatures were not determined for the present steels, they can be estimated to be in the vicinity of 650 °C. Thus, the simulations involved cooling down to about halfway through the intercritical range.) As indicated above, this can contribute to austenite grain refinement. In order to examine this effect, a variant of the S schedule was also performed in which the temperature was *not* allowed to cross the $A_{r3}$ before reheating.

The L size schedule, which is presented in Table II, differs from the S schedule in the following respects:

**Table II. L Simulation**

| Pass No. | Equivalent Strain per Pass | Temperature (°C) | Delay Time between Passes (s) |
|---|---|---|---|
| 1—piercer | 1.60 | 1230 | 54 |
| 2—MPM | 0.45 | 1085 | 1 |
| 3—MPM | 0.40 | 1072 | 1 |
| 4—MPM | 0.30 | 1060 | 0.5 |
| 5—MPM | 0.20 | 1050 | 0.5 |
| 6—MPM | 0.18 | 1020 | 75 |
| Tube furnace | — | 1000 | 5 |
| 7—SRM | 0.05 | 1000 | 0.5 |

Note: Soaking temperature is 1250 °C for 15 min. Delay time between billet reheating furnace and piercer is 80 s. The strain rate is 2 $s^{-1}$ for each pass.

(1) After the MPM, the specimen temperature does not drop below the $A_{r3}$, only decreasing to ~950 °C before reheating to 1000 °C.
(2) Only a single pass of 0.05 strain is given after exiting from the tube furnace, as opposed to a total strain of 1.6 applied in 16 passes.

Cooling rates after the SRM (between 800 °C and 500 °C) were ~3.5 °C/s and 1 °C/s for the S and L sizes, respectively. To clarify the influence of cooling rate on the S schedule, a further S variant was performed with a 1 °C/s cooling rate.

### B. *Materials and Testing Procedure*

The compositions and carbon equivalents of the steels are given in Table III. The Ti, V, and N levels are based on alloys designed for RCR processing;[9,16] the higher C and V concentrations were selected to produce higher as-hot-rolled yield strengths. The steels, which were supplied by the Metals Technology Laboratories, CANMET, were laboratory cast in permanent iron molds of section size 125 mm × 150 mm. Torsion specimens of 20-mm gage length and 6.4-mm diameter were machined from the ingots and subjected to multistage torsion tests, conducted in an argon atmosphere, using the schedules described above. The S simulation was also performed on a selection of currently rolled steel chemistries so that the rolling loads pertaining to the new steels could be estimated from the high-temperature flow stresses of the current steels. The torsion testing equipment and methods have been described elsewhere.[17]

After simulation, the specimens were retested in torsion at room temperature in order to assess the yield strengths associated with the as-hot-rolled microstructures. Finally, the simulation specimens were polished and etched with 2 pct nital to reveal the final microstructure just below the surface. The ferrite grain sizes and volume fractions of the nonferritic phase were determined by the intercept method and by point counting, respectively.

## III. RESULTS

### A. *Flow Resistance during Hot Deformation*

The stress-strain curves pertaining to passes 1 through 6, *i.e.*, to the piercer and MPM, are displayed in Figure 1 for the 10C-10V and 12C-16V steels. The equivalent strain to be applied to the surface of the torsion specimen was determined from the von Mises equation, as described earlier. The von Mises equivalent stress at the surface was calculated from the torque by conventional methods.[18] The latter was not used to calculate mill loads directly but to rank the loads expected for candidate steels relative to a standard steel of known load. The flow curve for the piercer (pass 1) increases to a maximum and then decreases to a plateau at the end of the pass. Such "single peak" behavior indicates the occurrence of dynamic recrystallization, which produces grain refinement in this case.[19] Curves 2 through 6, representing the passes given in the MPM, indicate almost complete softening between passes, *i.e.*, nearly complete static recrystallization. It is apparent from the two sets of curves that

**Table III. Chemical Composition and Carbon Equivalent (CE) of the Ti-V-N Steels in Weight Percent (N Content in Ppm)**

| Material | C | Si | Mn | S | P | Al | V | Ti | N | CE |
|---|---|---|---|---|---|---|---|---|---|---|
| 10C-10V | 0.10 | 0.30 | 1.70 | 0.008 | 0.013 | 0.014 | 0.10 | 0.010 | 150 | 0.42 |
| 18C-09V | 0.18 | 0.30 | 1.72 | 0.008 | 0.013 | 0.016 | 0.090 | 0.011 | 150 | 0.50 |
| 12C-16V | 0.12 | 0.37 | 1.70 | 0.008 | 0.014 | 0.019 | 0.16 | 0.013 | 200 | 0.45 |
| 19C-15V | 0.19 | 0.36 | 1.70 | 0.008 | 0.014 | 0.027 | 0.15 | 0.012 | 185 | 0.52 |

$$CE^* = C + F\left(\frac{Mn}{6} + \frac{Si}{24} + \frac{Cu}{15} + \frac{Ni}{28} + \frac{Cr + Mo + V + Nb + 5B}{5}\right)$$

*Per Canadian Standards Association Z245.1

increasing the V content from 0.10 to 0.16 wt pct increases the flow stress by about 10 pct. Other investigators have also observed that increasing the V level in microalloyed steels raises the resistance to hot deformation of the austenite.[20,21]

In Figure 2, the mean flow stress (MFS = area below the stress-strain curve divided by strain) values for passes 1 through 6 determined from the stress-strain curves are plotted against the inverse pass temperature for all the steel chemistries investigated. As expected, the MFS generally increases with decreasing pass temperature. The departures from this trend can be attributed to the variations in the strains applied in the different passes. For example,

(1) The rate of increase in the MFS when going from the piercer (pass 1) to the MPM (pass 2) is lower than the rate for MPM passes 2 and 3. This is a result of the much higher strain applied in the piercer pass (1.6) than in the MPM passes (~0.4).
(2) The decreases in MFS in passes 4 and 5 correspond to decreases in the strains applied in these passes (Table I).

Figure 2 confirms the observation that increasing the V level raises the resistance to hot deformation. By contrast, similar increases in the C concentration have almost no effect on the MFS.

Included in Figure 2 are the mean flow stresses associated with an Algoma grade containing 0.27C-0.16Cr, which is currently rolled in the #2 mill. The lower V steels exhibit MFS values which are comparable to the Algoma grade, thus indicating that the mill loads should be similar. The higher V steels, however, exhibit MFS values which are 10 to 15 pct greater. Such an increase in mill load is in the range that can be accommodated.[22]

Typical sets of stress-strain curves for the 10C-10V and 12C-16V steels deformed in the SRM part of the simulation are shown in Figure 3. As can be seen from Table I, the SRM finishing schedule is comprised of 16 passes, each of 0.1 equivalent strain with a 0.5 second interpass time between each pass. The stresses increase rapidly in the first three passes in both alloys; *i.e.*, there is strain accumulation with very little recrystallization during the short interpass times in these passes. However, as the number of passes increases beyond the fourth pass, the rate of stress increase is substantially reduced. This flow stress behavior can be interpreted more clearly by plotting the MFS values against inverse pass temperature, as illustrated in Figure 4. As will be shown in the Discussion, the point at which the rate of flow stress increase is drastically reduced indicates the onset of dynamic recrystallization, which is accompanied by some static softening between passes. It should be noted that the temperature decreases from 1000 °C to 840 °C during the SRM simulation. Therefore, part of the pass-to-pass

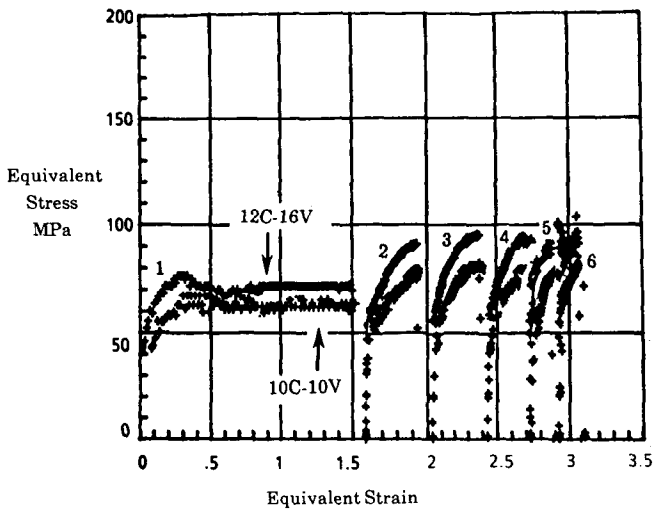


Fig. 1—Typical hot torsion simulation results for the piercer (curve 1) and MPM (curves 2 through 6).

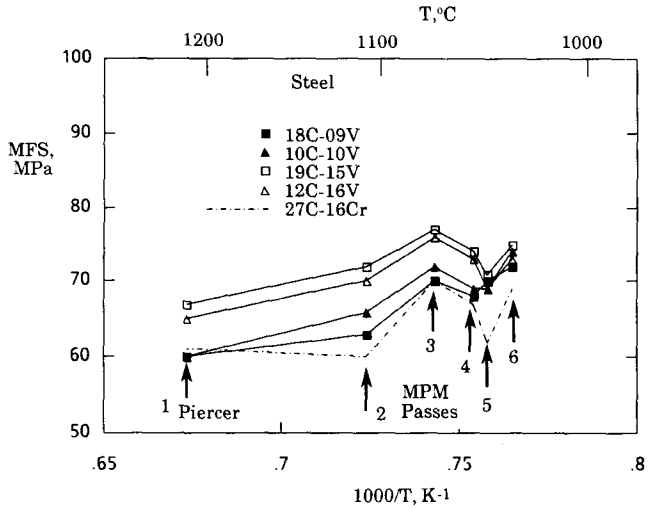


Fig. 2—Dependence of the mean flow stress on inverse pass temperature for simulation of the piercer and MPM. Data for a currently rolled grade (0.27C-0.31Si-1.21Mn-0.08Mo-0.16Cr) are shown for comparison. Note that the MFS scale begins at 50 MPa.

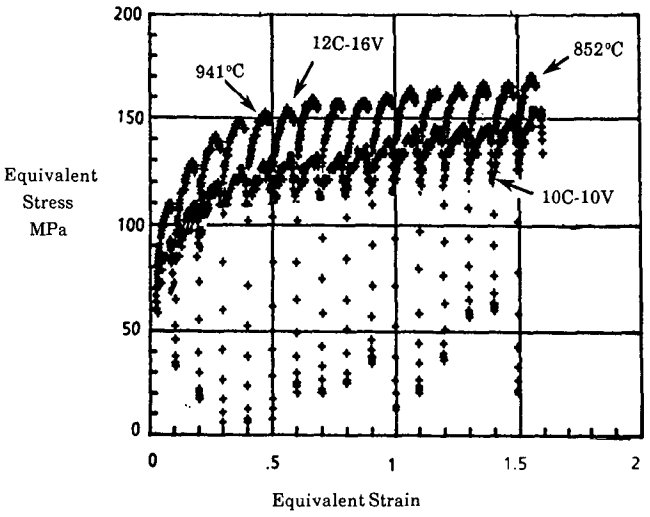


Fig. 3—Typical hot torsion simulation results for the SRM passes. Note that there is only a slight increase in flow stress after the fifth pass, even though the temperature is dropping steadily.

increase in flow resistance during the SRM simulation is attributable to this temperature drop. Finally, it should be noted that the results again show that increasing the V concentration raises the MFS, while similar increases in the C content have almost no effect.

Figure 4 also shows the data obtained for two currently rolled quench-and-temper chemistries. The MFS values for the lower V steels lie between those pertaining to the heat treatable chemistries, while the corresponding values for the higher V steels are 5 to 15 pct higher than those associated with current chemistries.

### B. *Microstructure after Hot Rolling*

Increasing the C content raises the volume fraction of the nonferritic phase, as can be seen by comparing Figures 5 and 6 (lower V) or Figures 7 and 8 (higher V). The nonferritic phase is predominantly pearlite in the lower C chemistries, but at the higher C levels, particularly in the 19C-15V chemistry, a significant volume fraction of bainite is evident (Figure 8).

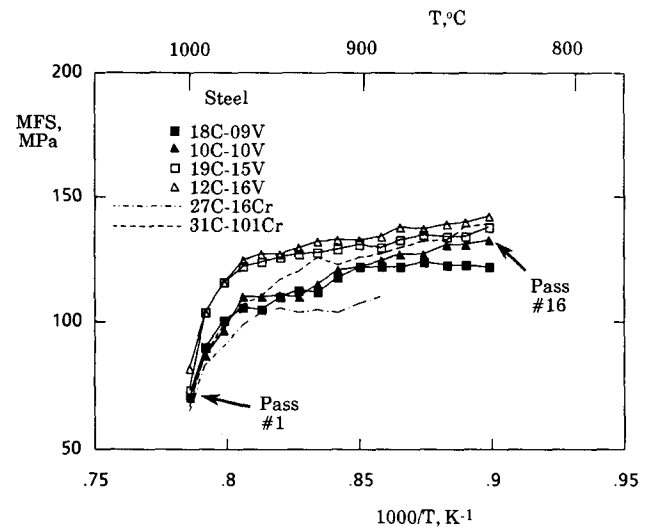


Fig. 4—Dependence of the mean flow stress on inverse pass temperature for the SRM simulations. Data for two currently rolled Algoma chemistries are shown for comparison. The full chemistry for the 31C-101Cr grade is 0.31C-0.27Si-0.79Mn-0.32Mo-1.01Cr. Note that the MFS scale begins at 50 MPa.

Figures 5(a) and (b) illustrate the final microstructures obtained in the 10C-10V chemistry after the size L and size S simulations, respectively. It is clear that the size S simulation results in a much finer microstructure. This behavior is confirmed in Figures 6 through 8 for the other chemistries studied, *i.e.*, the 18C-09V, 12C-16V, and 19C-15V grades, respectively.

In Tables IV(a) and (b), the microstructures shown in Figures 5 through 8 are described quantitatively in terms of the ferrite grain size and volume fraction of the nonferritic phase. This table confirms the observations described above. In addition, the detailed analysis indicates that increasing the C level is more effective in refining the ferrite grain size than a similar increase in the V content.

The grain refinement associated with the S simulation is largely due to dynamic recrystallization of the austenite during the SRM stage, as will be shown in more detail below. However, crossing the $A_{r3}$ temperature before entering the tube furnace and the faster cooling rate during the austenite-to-ferrite transformation also favor grain refinement. As mentioned earlier, the effect of the latter

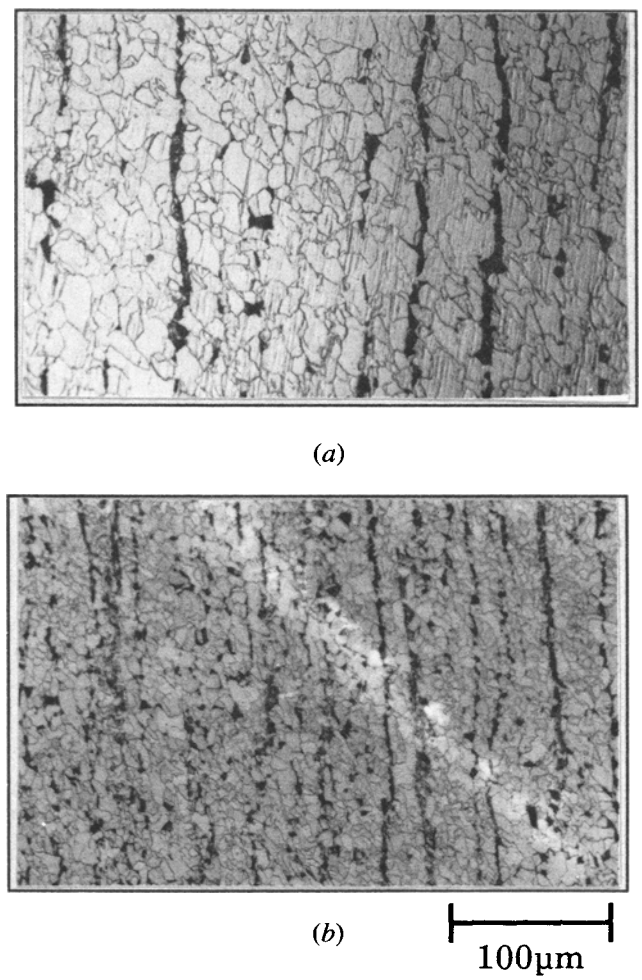


Fig. 5—Final microstructures for the 10C-10V chemistry, after the (*a*) L and (*b*) S simulations.

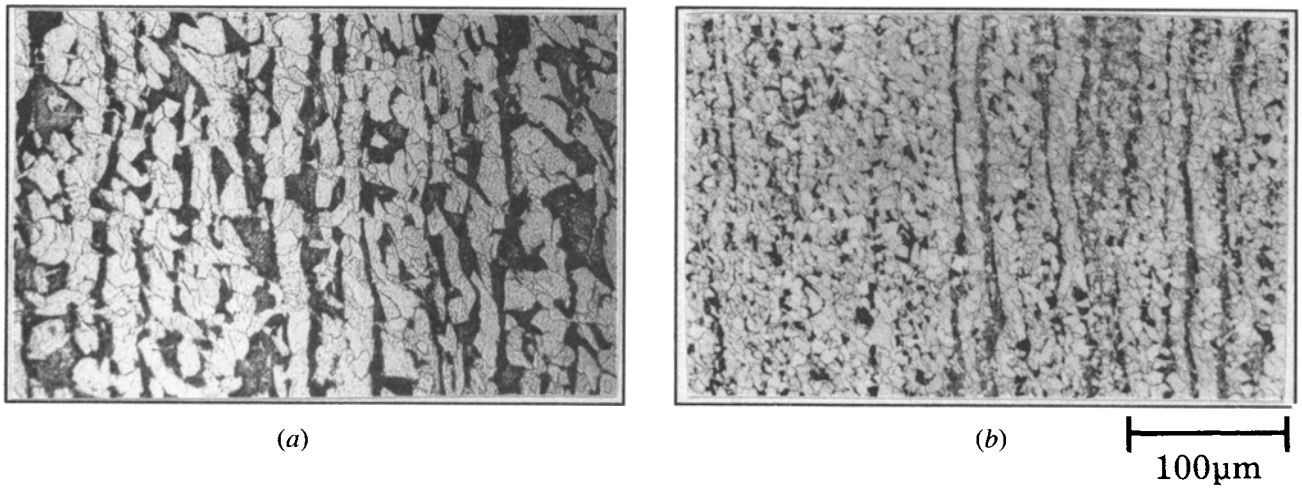


Fig. 6—Final microstructures for the 18C-09V chemistry, after the (*a*) L and (*b*) S simulations.

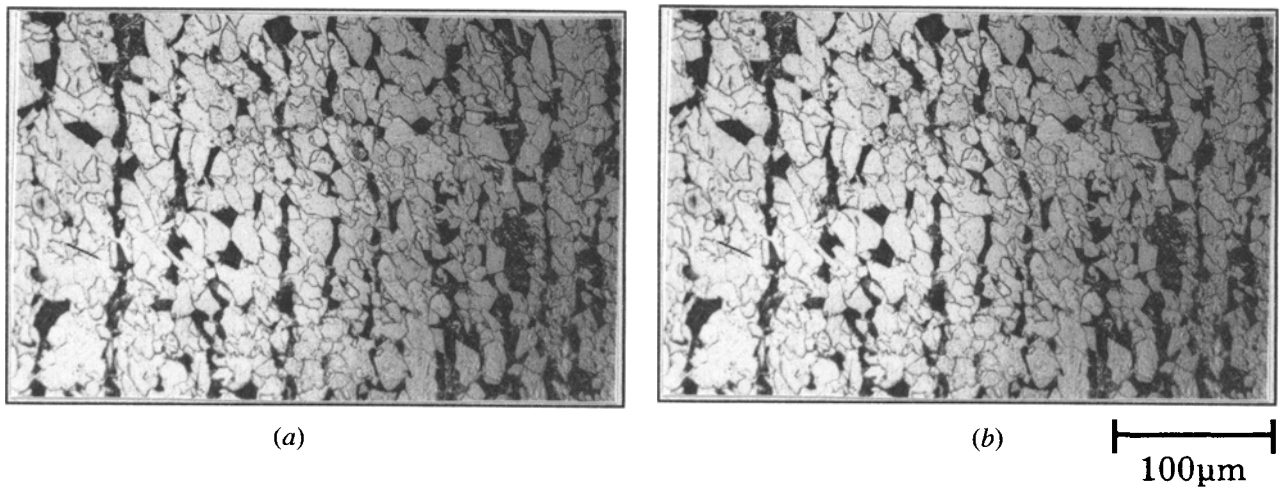


Fig. 7—Final microstructures for the 12C-16V chemistry, after the (*a*) L and (*b*) S simulations.

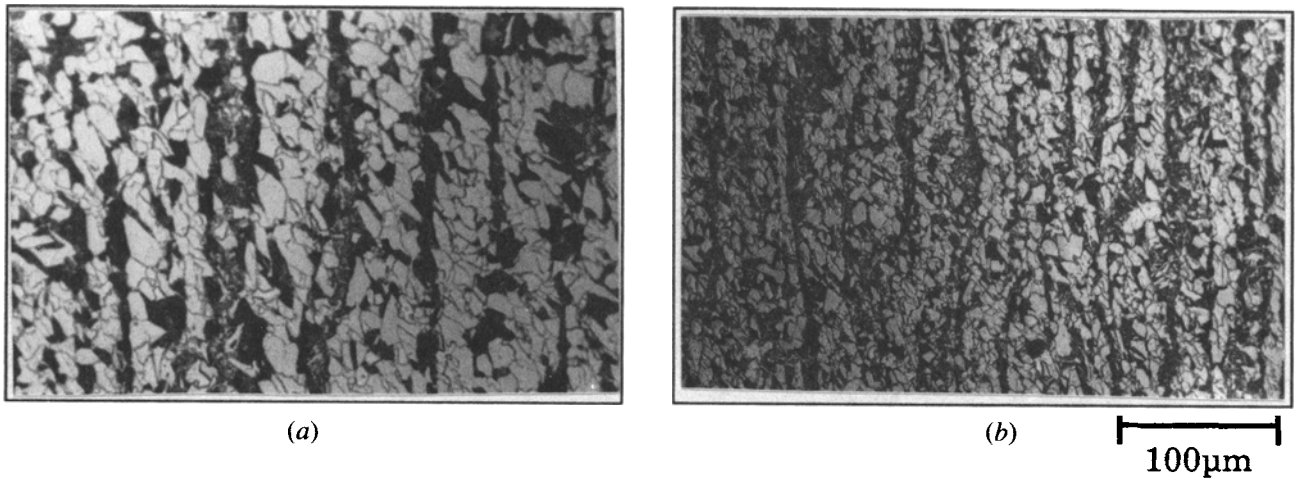


Fig. 8—Final microstructures for the 19C-15V chemistry, after the (*a*) L and (*b*) S simulations.

**Table IV. Relationship between Chemistry, Microstructure, and Yield Stress for S and L Simulations**

| Chemistry | Ferrite Grain Size μm | Ferrite Grain Size ASTM No. | Volume Fraction of Nonferritic Phase** (Pct) | Tensile Yield Stress* (MPa) |
|---|---|---|---|---|
| (a) Simulation of Size L | | | | |
| 10C-10V | 11.3 | 9.7 | 10.7 ± 1.5 (P) | 533 |
| 18C-09V | 9.8 | 10.1 | 33.9 ± 3.7 (P) | 624 |
| 12C-16V | 10.7 | 9.8 | 18.1 ± 3.2 (P) | 566 |
| 19C-15V | 9.7 | 10.1 | 25.6 ± 3.3 (P) | 728 |
| | | | 11.6 ± 3.7 (B) | |
| (b) Simulation of Size S | | | | |
| 10C-10V | 7.7 | 10.8 | 10.2 ± 2.3 (P) | 549 |
| 18C-09V | 6.8 | 11.1 | 32.3 ± 2.6 (P) | 629 |
| 12C-16V | 7.6 | 10.8 | 13.7 ± 2.8 (P) | 607 |
| 19C-15V | 6.6 | 11.2 | 34.9 ± 5.0 (P) | 715 |
| | | | 6.7 ± 3.2 (B) | |

*Estimated from room temperature torsion tests[23]
**P = pearlite, B = bainite

two factors was examined using the following variations of the size S simulation:

(1) *not* crossing the $A_{r3}$ temperature before entry to the tube furnace (Figure 9),
(2) decreasing the cooling rate from ~3.5 °C to ~1 °C/s (Figure 10), and
(3) a combination of (1) and (2) (Figure 11).

Generally, these micrographs show that cooling to 50 °C below the $A_{r3}$ does not cause any appreciable refinement (compare Figures 10 and 11), while the faster cooling rate does indeed produce grain refinement (compare Figures 9 and 11).

The quantitative features of Figures 9 through 11 are listed in Tables V(a) through (c). Comparison of Table IV(b) with V(a) and V(b) with V(c) confirms that the routine 50 °C cool below the $A_{r3}$ temperature before entry into the tube furnace does not significantly reduce the ferrite grain size. Comparing Table IV(b) with V(b) and V(a) with V(c) again shows that the faster cooling rate produces the finer ferrite grain size. This effect is most significant for the 10C-10V chemistry and negligible for the 19C-15V chemistry. Thus, two factors in

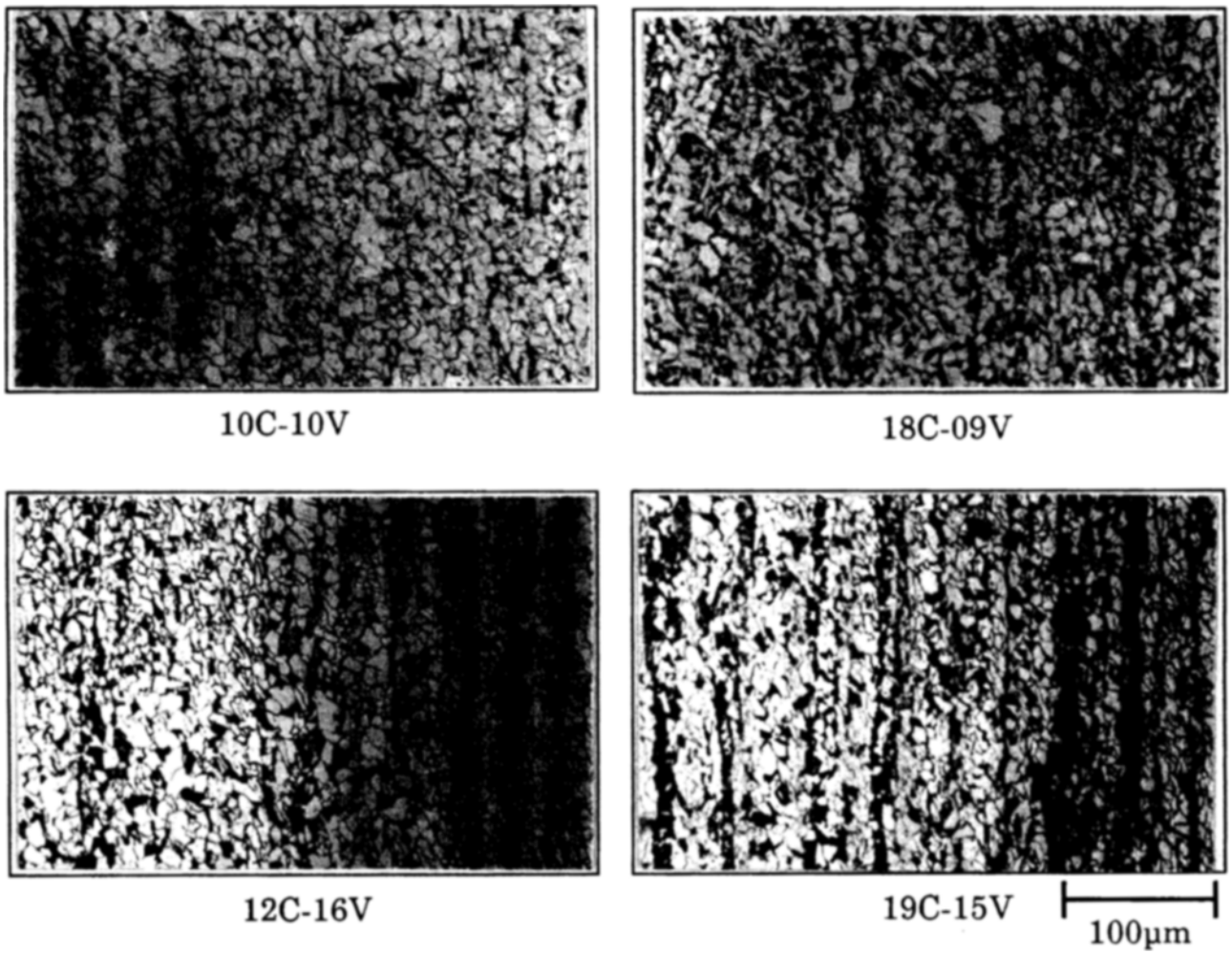


Fig. 9—Final size S microstructures after simulation without crossing the $A_{r3}$ temperature before entry to the intermediate reheat furnace. Samples were cooled after the SRM at ~3.5 °C/s.

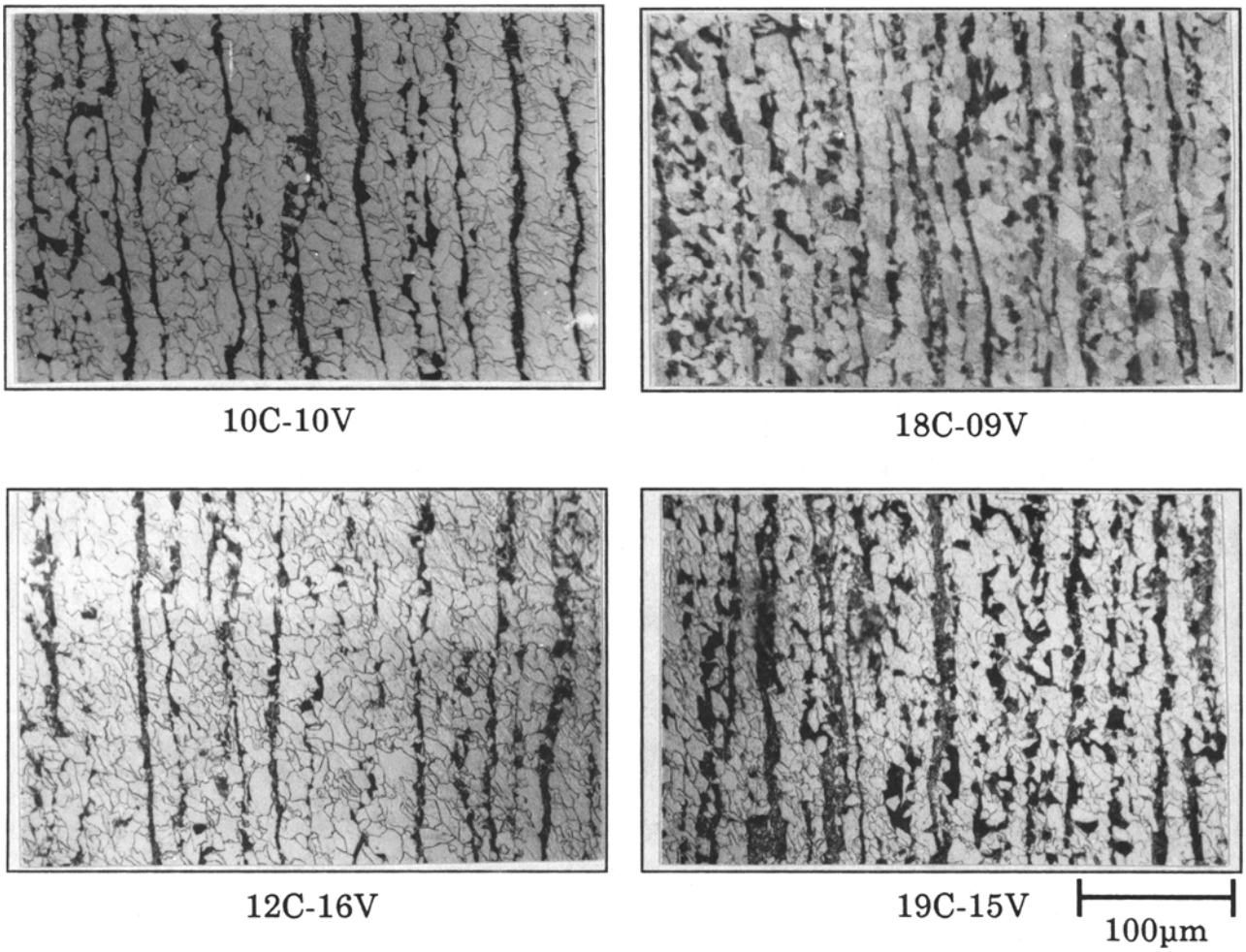


Fig. 10—Final size S microstructures after simulation with cooling to about 50 °C below the $A_{r3}$ temperature before entry to the reheat furnace. Samples were cooled after the SRM at ~1 °C/s.

the S schedule favor the production of finer ferrite microstructures:

(1) more SRM deformation, combined with a lower finishing temperature and
(2) a faster cooling rate during the austenite-to-ferrite transformation.

The magnitudes of these factors can now be quantified separately. For example, the greater SRM deformation reduces the ferrite grain size from 11.3 to 9.4 $\mu$m in the 10C-10V chemistry (compare Table IV(a) with V(c)). Increasing the cooling rate during transformation leads to a further refinement to 8.1 $\mu$m (Table V(a)), while cooling to 50 °C below the $A_{r3}$ reduces the ferrite grain size very slightly to 7.7 $\mu$m (Table IV(b)). In the case of the 19C-15V chemistry, the greater SRM deformation reduces the ferrite grain size from 9.7 to 7.0 $\mu$m, increasing the cooling rate reduces it to 6.6 $\mu$m, and the routine cooling below the $A_{r3}$ has no effect at all.

### C. *Room-Temperature Yield Strength*

The room-temperature yield strengths in *tension* were estimated from an empirical relationship between the tensile and torsional yield strengths.[23] Both sets of yield stresses are summarized in Table VI for the size L simulations. With respect to chemistry, the results show that increasing the C concentration raises the yield strength to a greater degree than increasing the V content. As noted in the previous section, increasing the C level is apparently more effective in refining the ferrite grain size than a similar increase in the V content. This, plus the increase in the volume fraction of the nonferritic phase, leads to the apparently greater strengthening effect of C over V.

The room-temperature yield strengths after the size S simulation and simulation variants are summarized in Table VII. If a particular chemistry is considered, *e.g.*, 19C-15V, it can be seen that

(1) increasing the cooling rate from ~1 °C to ~3.5 °C/s is effective in raising the yield strength and
(2) crossing the $A_{r3}$ temperature and cooling to ~680 °C does not significantly increase the yield strength.

These observations are consistent with the microstructural findings and are generally valid for the other chemistries investigated.

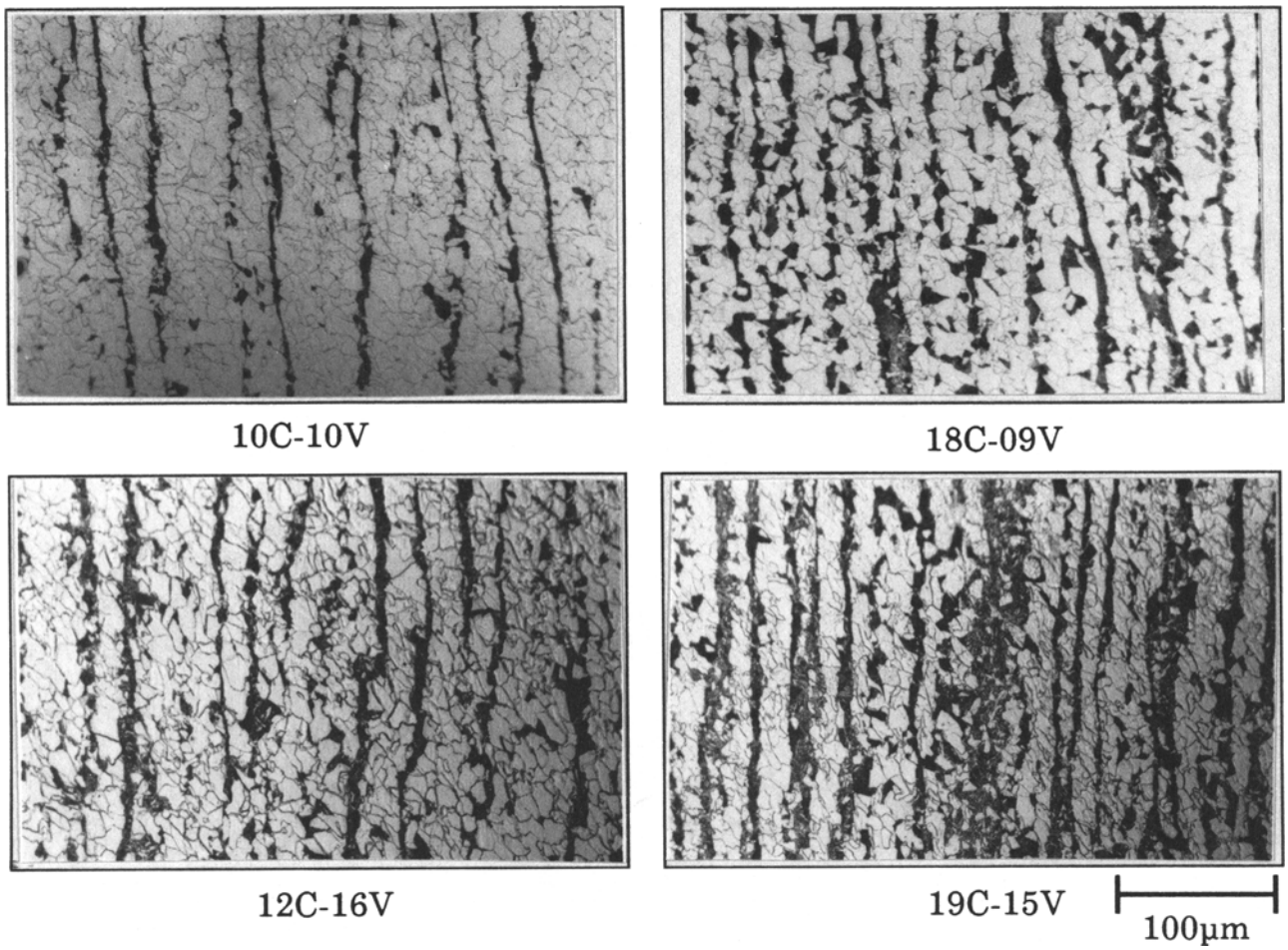


Fig. 11—Final size S microstructures after simulation without crossing the $A_{r_3}$ temperature before entry to the reheat furnace. Samples were cooled after the SRM at ~1 °C/s.

## IV. DISCUSSION

### A. *Flow Resistance during Hot Rolling*

The pass-to-pass variation in MFS reveals changes that are occurring in the microstructure during hot deformation. Since these changes influence the final room-temperature microstructure, it is of interest to analyze the MFS results in terms of the evolution of the austenite microstructure. The first six passes, which correspond to the RCR schedule, reveal little, apart from the fact that full or nearly full recrystallization occurs after each pass. Of greater interest is the finishing (SRM) stage in the S schedule.

During SRM rolling, there is strain accumulation up to the third pass followed by partial softening after the fourth pass, as indicated by the decrease in the rate of stress increase (Figures 3 and 4). Since appreciable static recrystallization takes longer than 0.5 seconds at these temperatures (950 °C to 840 °C),[24] dynamic recrystallization is the principal softening mechanism from the fourth pass onward, accompanied by some postdynamic recrystallization. As a result, the flow stresses rise only slowly during SRM rolling, despite the drop in temperature.

This can be seen more clearly by taking the flow curves of Figure 3 (which were determined at a series of *decreasing* temperatures) and replotting them at a constant "standardized" temperature of 905 °C. The temperature dependence of the MFS, $\bar{\sigma}$, (*i.e.*, the yield stress and low strain flow stress) for these steels is given by

$$\bar{\sigma}\,(\text{MPa}) = -268 + 4.55 \times 10^5/T\,(\text{K})$$

Using this equation, the change in flow stress, $\Delta\sigma$, due to temperature change, $\Delta T$, was calculated and applied to the flow curves for the 12C-16V chemistry. The "corrected" flow curves are shown in Figure 12. These are the curves that would have been obtained had the SRM deformation been applied at a constant temperature. The envelope of these flow curves shows the "single peak" behavior characteristic of dynamic recrystallization, which produces grain refinement in the present case.[19] This confirms that dynamic recrystallization is taking place during SRM deformation.

The "rounding" of the flow curves pertaining to the individual passes in Figure 12 is due to a combination of static recovery and postdynamic recrystallization.[24] Note, however, that due to the short interpass times (0.5 seconds), there is only limited softening produced by this type of recrystallization. Such behavior is opposite to the low-temperature behavior of Nb steels in

**Table V. Relationship between Chemistry, Microstructure, and Yield Stress after Process Route Variations of the S Simulation**

| Chemistry | Ferrite Grain Size μm | Ferrite Grain Size ASTM No. | Volume Fraction of Nonferritic Phase** (Pct) | Tensile Yield Stress* (MPa) |
|---|---|---|---|---|
| (a) Processing Route Variant: without Crossing the $A_{r3}$ | | | | |
| 10C-10V | 8.1 | 10.6 | 10.0 ± 1.6 (P) | 549 |
| 18C-09V | 6.8 | 11.1 | 31.6 ± 4.3 (P) | 589 |
| 12C-16V | 7.5 | 10.8 | 14.8 ± 1.9 (P) | 637 |
| 19C-15V | 6.6 | 11.2 | 30.3 ± 3.5 (P) | 715 |
| | | | 6.1 ± 3.0 (B) | |
| (b) Processing Route Variant: Cooling Rate (800 °C to 500 °C) ~ 1 °C/s | | | | |
| 10C-10V | 10.3 | 9.9 | 13.8 ± 2.6 (P) | 497 |
| 18C-09V | 8.1 | 10.6 | 28.5 ± 2.8 (P) | 569 |
| 12C-16V | 10 | 10.0 | 13.3 ± 2.9 (P) | 546 |
| 19C-15V | 6.9 | 11.1 | 37.8 ± 3.6 (P) | 637 |
| (c) Processing Route Variant: without Crossing the $A_{r3}$, Cooling Rate (800 °C to 500 °C) ~ 1 °C/s | | | | |
| 10C-10V | 9.4 | 10.2 | 11.2 ± 2.8 (P) | 468 |
| 18C-09V | 7.3 | 10.9 | 33.1 ± 3.8 (P) | 572 |
| 12C-16V | 9.3 | 10.2 | 16.2 ± 2.9 (P) | 533 |
| 19C-15V | 7.0 | 11.0 | 34.5 ± 3.3 (P) | 624 |

*Estimated from room temperature torsion tests[23]
**P = pearlite, B = bainite

reversing mills in which austenite pancaking takes place instead.[10,11] In the present schedule, however, the interval between SRM passes in only 0.5 seconds, which is insufficient for copious precipitation.[25] Moreover, of the strong carbonitride-forming elements, V is recognized as being the weakest in terms of promoting the pancaking of austenite.[20,26,27] Thus, in the absence of sufficient precipitation for pancaking and in the presence of solutes which delay static recrystallization, the critical strain for dynamic recrystallization is readily attained.

In Figure 13, a schematic diagram is presented together with a set of MFS values reproduced from Figure 4. Here, three straight lines can be seen, the lowest of which is associated with static recrystallization. This line applies to RCR rolling (at constant pass strains of about 0.4) and, therefore, to certain regions of the MPM where such conditions are satisfied. It could only be valid for the SRM if there were full recrystallization or softening between passes. The slope of the line representing static recrystallization is $\sim 4 \times 10^5$ MPa K, which is similar to the slope between MPM passes 2 and 3 or 5 and 6, shown in Figure 2. The steepest line (slope $\sim 20 \times 10^5$ MPa K) corresponds to the "strain accumulation" which takes place in the first three passes of the SRM. When accompanied by sufficient precipitation, as in reversing mills, strain accumulation continues to take place as the temperature decreases, leading to pancaking of the austenite (*i.e.*, to conventional "controlled rolling"). In the absence of sufficient precipitation, the critical strain for dynamic recrystallization is attained, and the rate of flow stress increase drops to about $2 \times 10^5$ MPa K, that is, to values below those pertaining to static recrystallization. The "dynamic" line is located above the "static" line because of the strain accumulation required to initiate (and maintain) the dynamic recrystallization process.

**Table VI. Room-Temperature Yield Strengths after L Simulations**

| Chemistry | Yield Stress Torsion (MPa) | Yield Stress Tension (MPa)* | Yield Stress Tension (ksi)* | Flow Curve Type |
|---|---|---|---|---|
| 10C-10V | 410 | 533 | 77 | DC |
| 18C-09V | 480 | 624 | 91 | C |
| 12C-16V | 435 | 566 | 82 | C |
| 19C-15V | 560 | 728 | 106 | C |

Note: The flow curves measured at room temperature displayed either discontinuous (DC) or continuous (C) yielding in torsion.
*Estimated from room temperature torsion tests.[23]

### B. *Microstructure-Mechanical Property Relationships*

When comparing the microstructures and yield strengths for the size L and size S simulations (Tables IV(a) and (b)), it is notable that for a specific chemistry, the grain size due to the S schedule is much finer than for the L schedule, but there is no significant difference in the volume fractions of the nonferritic phase. However, such grain refinement does not lead to increased room-temperature yield strengths, indicating that the L schedule generates more precipitation hardening of the ferrite than the S schedule and compensates for the coarser grain size in this way.

In the chemistries investigated, the precipitating species of interest during rolling is VN. (The precipitation of TiN is completed at temperatures above 1250 °C and can thus be disregarded during rolling.) The solubility equation for VN precipitation,[28] *i.e.*,

$$\log [V] [N] = 3.46 - 8330/T$$

reveals that VN precipitation is not expected to take place during the MPM stage of rolling but may occur before or during SRM deformation. The VN solution temperatures for the four steels calculated from the above relation are listed in Table VIII. Given that strain-induced precipitation is generally observed at about 100 °C or more below the respective solution temperature,[26] such precipitation is expected to occur below 1000 °C and 925 °C in the high and low V chemistries, respectively. Vanadium-containing precipitates have been observed by scanning transmission electron microscope (STEM) analysis in supersaturated deformed austenite by other investigators.[29] Increasing the V concentration to 0.2 wt pct in microalloyed steels containing 0.016 wt pct N has resulted in an increased density of precipitates in deformed austenite[30] and retards recrystallization.[20]

Due to the small strain applied at 1000 °C in the SRM when simulating the L size, little precipitation of VN will take place in the austenite, leading to substantial V(CN) precipitation in the ferrite. By contrast, some strain-induced precipitation is likely to take place in the deformed austenite in the SRM as a result of the 1.6

**Table VII. Room-Temperature Yield Strengths after S Simulations and Their Variants**

| Chemistry | Processing Route | Yield Stress Torsion (MPa) | Yield Stress Tension (MPa)* | Yield Stress Tension (ksi)* | Flow Curve Type |
|---|---|---|---|---|---|
| 10C-10V | XAC | 382 | 497 | 72 | DC |
| 10C-10V | XACC | 422 | 549 | 80 | DC |
| 10C-10V | WXAC | 360 | 468 | 68 | DC |
| 10C-10V | WXACC | 422 | 549 | 80 | DC |
| 18C-09V | XAC | 438 | 569 | 83 | DC |
| 18C-09V | XACC | 484 | 629 | 91 | C |
| 18C-09V | WXAC | 440 | 572 | 83 | DC |
| 18C-09V | WXACC | 453 | 589 | 85 | C |
| 12C-16V | XAC | 420 | 546 | 79 | DC |
| 12C-16V | XACC | 467 | 607 | 88 | C |
| 12C-16V | WXAC | 410 | 533 | 77 | DC |
| 12C-16V | WXACC | 490 | 637 | 92 | C |
| 19C-15V | XAC | 490 | 637 | 92 | C |
| 19C-15V | XACC | 550 | 715 | 104 | C |
| 19C-15V | WXAC | 480 | 624 | 91 | C |
| 19C-15V | WXACC | 550 | 715 | 104 | C |

Note: Processing was carried out with (X) or without (WX) crossing the $A_{r3}$. Specimens were cooled from 800 °C to 500 °C after the SRM at rates of ~1(AC) °C or ~3.5(ACC) °C/s.
*Estimated from room-temperature torsion tests.[23]

strain that is applied in the S schedule at the lower temperatures. Therefore, less V(CN) precipitation is expected to take place in the ferrite in this case. Similar observations have been reported by others investigating the effects of thermomechanical processing on precipitation strengthening in HSLA steels containing V and N.[31]

In Table IX, the results of microhardness testing of the ferrite are shown. Clearly, the larger grain size material produced by the size L simulation has a higher hardness than the smaller grain size material produced by the size S simulation. This indicates that there is more precipitation hardening of the ferrite in the size L than in the size S simulation. The above observations are in agreement with recent work on Ti-V microalloyed steels, where higher finish-rolling temperatures produced more precipitation strengthening of the ferrite compared to lower finish-rolling temperatures.[32] Similar trends have been reported for other microalloyed steels.[33]

Finally, it should be pointed out that although the S and L simulations lead to nearly the same yield strengths for a specific chemistry, size S will have superior toughness due to the finer ferrite grain size and smaller degree of precipitation hardening of the ferrite and, therefore,

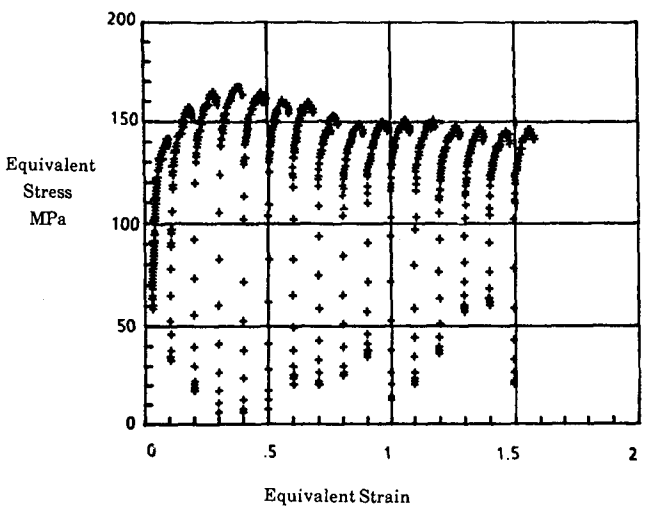


Fig. 12—SRM pass flow curves for the 12C-16V steel, corrected to a constant temperature of 905 °C. Note that the flow curve envelope displays the "single peak" behavior characteristic of dynamic recrystallization, which produces grain refinement in the present case.

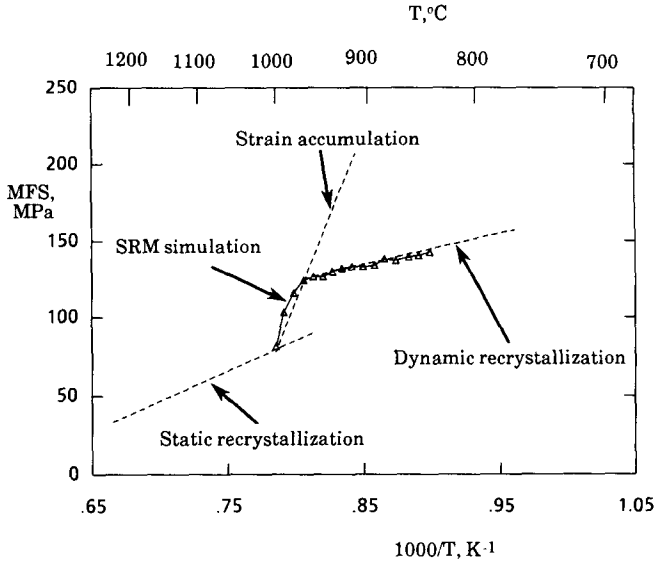


Fig. 13—Schematic representation of the dependence of MFS, determined for a constant pass strain, on inverse pass temperature. The data points represent the 16-pass schedule applied to the 12C-16V grade shown in Fig. 4, with pass strains of 0.1 and interpass delays of 0.5 s. The cooling rate used was ~10 °C/s. The temperature dependencies associated with static recrystallization (lower left), strain accumulation (upper center), and dynamic recrystallization (lower right) are shown.

**Table VIII. VN Solution Temperatures**

| Chemistry | V/N Atom Ratio* | Solution Temperature* (°C) |
|---|---|---|
| 10C-10V | 2.27 | 1033 |
| 18C-09V | 2.01 | 1022 |
| 12C-16V | 2.71 | 1105 |
| 19C-15V | 2.75 | 1091 |

*Based on the N available subsequent to the precipitation of TiN

is a more attractive schedule. (An increase in strength can be achieved by raising the volume fraction of the nonferritic phase, but this will also cause a deterioration in toughness.)

### C. *The Effect of Chemistry and Processing Variables on Microstructure*

It has been observed that for a particular processing route, raising the C content is more effective than raising the V content in refining the ferrite grain size. This is probably due to the superior effect of C in solution in the austenite in lowering the $A_{r3}$ temperature, which increases the austenite-to-ferrite grain size ratio.[32,34] Another factor is that the growth of ferrite is terminated at an earlier stage for the higher C chemistry due to the larger volume fraction of pearlite. Finally, increasing the cooling rate from ~1 °C to ~3.5 °C/s when simulating the S size produces further ferrite grain refinement due to supercooling.

Although cooling the tube to 50 °C below the $A_{r3}$ temperature before entry to the intermediate reheat furnace, in principle, should contribute to austenite grain refinement, it was not effective in the S schedule. This may be due to the subsequent austenite grain refinement caused by the substantial SRM deformation, which may have masked any refinement due to the above process variant. However, in the larger tube sizes, where the SRM deformation is small, the effect of this treatment may be significant. To increase the effectiveness of this technique, cooling to still lower temperatures, sufficient to cross *both* the $A_{r3}$ and the $A_{r1}$, is a possibility which is currently under examination.

**Table IX. Ferrite Microhardness in the Final Microstructures**

| Chemistry | Ferrite Grain Size ($\mu$m) | Microhardness ($DPH_{25gr}$) |
|---|---|---|
| (a) Simulation of Size L, Cooling Rate (800 °C to 500 °C) ~ 1 °C/s | | |
| 10C-10V | 11.3 | 225 ± 4 |
| 12C-16V | 10.7 | 226 ± 8 |
| (b) Variation of Size S Simulation, *i.e.*, Cooling Rate (800 °C to 500 °C) ~ 1 °C/s | | |
| 10C-10V | 10.3 | 201 ± 7 |
| 10C-10V* | 9.4 | 197 ± 5 |
| 12C-16V | 10.0 | 210 ± 4 |
| 12C-16V* | 9.3 | 209 ± 6 |

*Without crossing the $A_{r3}$

The nonferritic phase is a major source of strengthening, and the exact nature of this microstructural component significantly affects both the strength and toughness of the microstructure. In the initial stages of the austenite-to-ferrite transformation, polygonal ferrite is formed, and at the later stages of the transformation, the remaining austenite is enriched in C and transforms mainly to pearlite. But if the austenite contains sufficient Mn and/or V, it may transform to bainite. Furthermore, a larger austenite grain size and a faster cooling rate all tend to increase the possibility of the austenite-to-bainite transformation. For example, the 19C-15V chemistry contains bainite when a large austenite grain size (size L simulation) is subjected to a cooling rate of ~1 °C/s *or* when a small austenite grain size (size S simulation) is cooled at ~3.5 °C/s. However, in the latter case, when the cooling rate is reduced to ~1 °C/s, bainite was not observed (Tables IV and V).

## V. CONCLUSIONS

A series of Ti-V-N microalloyed steels was subjected to torsional simulation of a seamless tube hot-forming process. The major conclusions of this work are the following:

1. Increasing the V level from 0.1 to 0.15 pct leads to a 5 to 15 pct increase in the resistance to hot deformation, the exact increase depending on the details of thermomechanical processing.
2. Increasing the C concentration increases grain refinement and also raises the volume fraction of the nonferritic phase. The combined effect of these two factors increases the yield strength more effectively than raising the V content to a similar degree.
3. For a specific chemistry, the S schedule produces significantly finer ferrite grain sizes than the L schedule. The room-temperature yield strengths, however, are not affected by such a schedule variation. This results from the increased amount of precipitation hardening taking place in the *ferrite* (as opposed to the austenite) in the L schedule due to the limited low-temperature deformation applied in the latter case.
4. The finer microstructures resulting from the S schedule are due to (1) relatively high SRM deformation, leading to dynamic recrystallization, (2) the lower finishing temperature, and (3) the faster cooling rate during the austenite-to-ferrite transformation.
5. When simulating the S size, cooling to 50 °C below the $A_{r3}$ before entry to the intermediate reheat furnace is not effective in producing ferrite grain refinement because of the strong influence of the factors outlined in (4).
6. For the size S schedule, increasing the cooling rate from ~1 °C to ~3.5 °C/s during transformation results in a finer ferrite grain size, which leads to grain size strengthening.
7. The simulations produced fine-grained ($\leqq$11 $\mu$m) ferrite-pearlite microstructures with as-hot-rolled yield strengths in the range of 483 to 698 MPa (70 to 100 ksi). Yield strengths greater than 698 MPa (100 ksi) were obtained from partially bainitic microstructures.

## ACKNOWLEDGMENTS

The authors are indebted to the Algoma Steel Corporation for permission to publish this work. They also acknowledge with gratitude the financial assistance received from the following sources: the Algoma Steel Corporation, the Canadian Steel Industry Research Association, the Natural Sciences and Engineering Research Council of Canada, and the Quebec Ministry of Education (FCAR program). Thanks are also due to P.J. Hunt (Algoma Steel Corporation), Dr. G.E. Ruddle (Metals Technology Laboratories, CANMET), and Dr. R. Barbosa (Federal University of Minas Gerais, Brazil) for many helpful discussions. The steels were supplied by MTL, CANMET. LNP expresses his thanks to the University of Peradeniya for granting a period of sabbatical leave.

## REFERENCES

1. A. Reeder, C.G. Vasey, and D.J. Naylor: *Fundamentals of Microalloying Forging Steels*, TMS-AIME, Warrendale, PA, 1987, pp. 217-33.
2. J.R. Paules and S. Fisher: *30th Mechanical Working and Steel Processing Conf. Proc.*, Vol. XXVI, ISS-AIME, Warrendale, PA, 1988, pp. 59-64.
3. M. Korchynsky: *Mater. Eng.*, 1986, vol. 103 (10), pp. 45-48.
4. S. Yue, J.J. Jonas, and P.J. Hunt: *28th Mechanical Working and Steel Processing Conf. Proc.*, Vol. XXIV, ISS-AIME, Warrendale, PA, 1986, pp. 115-26.
5. R. Barbosa, S. Yue, J.J. Jonas, and P.J. Hunt: *Int. Conf. on Physical Metallurgy of Thermomechanical Processing of Steels and Other Metals (Thermec-88)*, I. Tamura, ed., Iron and Steel Inst. of Japan, Tokyo, 1988, pp. 535-42.
6. J.B. Code: *Iron & Steel Engineer*, 1987, vol. 64 (10), pp. 26-31.
7. W. Roberts, A. Sandberg, T. Siwecki, and T. Welefors: *HSLA Steels: Technology and Applications*, M. Korchynsky, ed., ASM, Metals Park, OH, 1984, pp. 67-84.
8. F.H. Samuel, S. Yue, J.J. Jonas, and B.A. Zbinden: *ISIJ International*, 1989, vol. 29, pp. 878-86.
9. T. Siwecki, A. Sandberg, and W. Roberts: *HSLA Steels: Technology and Applications*, M. Korchynsky, ed., ASM, Metals Park, OH, 1984, pp. 619-34.
10. F. Boratto, S. Yue, J.J. Jonas, and T.H. Lawrence: *Int. Conf. on Physical Metallurgy of Thermomechanical Processing of Steels and Other Metals (Thermec-88)*, I. Tamura, ed., Iron and Steel Inst. of Japan, Tokyo, 1988, pp. 519-26.
11. F. Boratto, S. Yue, and J.J. Jonas: United States Patent No. 4,840,051.
12. P. Choquet, A. Le Bon, and Ch. Perdrix: *Strength of Metals and Alloys*, H.J. McQueen, J.-P. Bailon, J.I. Dickson, J.J. Jonas, and M.G. Akben, eds., Pergamon Press, New York, NY, 1985, pp. 1025-30.
13. B. Migaud: *Hot Working and Forming Processes*, C.M. Sellars and G.J. Davies, eds., TMS, London, 1980, pp. 67-76.
14. T.Z. Blazynski and I.M. Cole: *Proc. Inst. Mech. Eng. (London)*, 1963–64, vol. 178, part I, pp. 867-93.
15. C. Ouchi, T. Sampei, and I. Kozasu: *Trans. ISIJ*, 1982, vol. 22, pp. 214-22.
16. G.E. Ruddle, D.L. Baragar, and A.F. Crawley: *26th Mechanical Working and Steel Processing Conf. Proc.*, vol. XXII, ISS-AIME, Warrendale, PA, 1984, pp. 183-95.
17. T. Chandra, S. Yue, and J.J. Jonas: *Proc. Conf. the Science and Technology of Flat Rolling*, Deauville, France, 1987, pp. F 18.1-F 18.8.
18. S.L. Semiatin, G.D. Lahoti, and J.J. Jonas: *ASM Metals Handbook*, vol. 8, 9th ed., ASM, Metals Park, OH, 1985, pp. 154-84.
19. J.J. Jonas: *Int. Conf. on Physical Metallurgy of Thermomechanical Processing of Steels and Other Metals (Thermec-88)*, I. Tamura, ed., Iron and Steel Inst. of Japan, Tokyo, 1988, pp. 59-69.
20. M.J. White and W.S. Owen: *Metall. Trans. A*, 1980, vol. 11A, pp. 597-604.
21. M.J. Crooks, A.J. Garratt-Reed, J.B. Vander Sande, and W.S. Owen: *Metall. Trans. A*, 1981, vol. 12A, pp. 1999-2013.
22. Algoma Steel Corporation, Sault Ste. Marie, ON, Canada, private communication, 1989.
23. S. Yue, F. Boratto, and J.J. Jonas: *Proc. Conf. on Hot and Cold-Rolled Sheet Steels*, Cincinnati, OH, 1987, R. Pradhan and G. Ludkovsky, eds., TMS-AIME, Warrendale, PA, 1988, pp. 349-59.
24. T. Sakai, M. Ohashi, K. Chiba, and J.J. Jonas: *Acta Metall.*, 1988, vol. 36, pp. 1781-90.
25. F.H. Samuel, R. Barbosa, F. Boratto, S. Yue, and J.J. Jonas: *Int. Conf. on Physical Metallurgy of Thermomechanical Processing of Steels and Other Metals (Thermec-88)*, I. Tamura, ed., Iron and Steel Inst. of Japan, Tokyo, 1988, pp. 721-28.
26. M.G. Akben, I. Weiss, and J.J. Jonas: *Acta Metall.*, 1981, vol. 29, pp. 111-21.
27. L.J. Cuddy: *Thermomechanical Processing of Microalloyed Austenite*, A.J. De Ardo, G.A. Ratz, and P.S. Wray, eds., TMS-AIME, Warrendale, PA, 1982, pp. 129-40.
28. K.J. Irvine, F.B. Pickering, and T. Gladman: *J. Iron Steel Inst.*, 1967, vol. 205, pp. 161-82.
29. J.G. Speer, J.R. Michael, and S.S. Hansen: *Metall. Trans. A*, 1987, vol. 18A, pp. 211-22.
30. J.R. Michael, J.G. Speer, and S.S. Hansen: *Metall. Trans. A*, 1987, vol. 18A, pp. 481-83.
31. R.K. Amin, M. Korchynsky, and F.B. Pickering: *Met. Technol.*, 1981, vol. 8, pp. 250-62.
32. T. Siwecki: *Int. Conf. on Physical Metallurgy of Thermomechanical Processing of Steels and Other Metals (Thermec-88)*, I. Tamura, ed., Iron and Steel Inst. of Japan, Tokyo, 1988, pp. 232-39.
33. J.C. Herman and V. Leroy: *Int. Conf. on Physical Metallurgy of Thermomechanical Processing of Steels and Other Metals (Thermec-88)*, I. Tamura, ed., Iron and Steel Inst. of Japan, Tokyo, 1988, pp. 283-90.
34. I. Tamura: *Int. Conf. on Physical Metallurgy of Thermomechanical Processing of Steels and Other Metals (Thermec-88)*, I. Tamura, ed., Iron and Steel Inst. of Japan, Tokyo, 1988, pp. 1-10.